

Hysteresis and Hydrodynamic Collapse in Leidenfrost Vapor Layers

Dana Harvey, Joshua Méndez Harper, and Justin C. Burton*
Department of Physics, Emory University, Atlanta, Georgia 30322, USA
(Dated: October 21, 2020)

During the Leidenfrost effect, a thin insulating vapor layer separates an evaporating liquid from a hot solid. Here we show that Leidenfrost vapor layers can be sustained at much lower temperatures than those required for formation. We use an electrical technique with microsecond resolution to measure the thickness of the vapor and find that explosive failure occurs at temperatures and thicknesses that do not depend on material and fluid properties, such as thermal conductivity or salinity, for smooth, metallic surfaces. Numerical simulations confirm that the hydrodynamic flow of the vapor determines the lowest possible temperature for maintaining stable Leidenfrost films.

In his seminal 1756 treatise, J. G. Leidenfrost noted that a water droplet placed on a heated, polished metal spoon does not wet the surface [1]. Instead, the water droplet levitates above the hot surface, cushioned by a vapor film generated by evaporation. Since then, the Leidenfrost effect has been well studied due to its importance in laboratory, industrial, and geophysical contexts [2]. Examples include the vapor layer geometry [3–8], spontaneous motion and oscillations of drops [9–15], drop impact on heated surfaces [16–19], and “nano-painting” through particle deposition [20, 21].

In nature, the Leidenfrost effect—or more precisely, the collapse of a Leidenfrost vapor layer between ascending magma and an aquifer—underpins one of the most energetic and common forms of volcanism: phreatomagmatic eruptions [22, 23]. The Leidenfrost effect need not involve water or even a liquid; blocks of sublimating CO₂ ice may “surf” down Martian dunes on lubricating layers of CO₂ gas, carving channels and pits on the red planet’s surface [24]. This very manifestation of the Leidenfrost effect may help power the first Martian colonies [25].

In all of these examples, precise knowledge of the transition temperature at which the vapor layer forms (or fails) is crucial. However, reported values of this temperature vary widely in the literature, and are known to depend on surface roughness [26–30], hydrophobicity [29, 31–33], thermal properties of the solid [32–37], liquid temperature [29, 34, 35, 37–39], solid geometry [32–35, 37, 38, 40, 41], and liquid impurities [29, 36, 41, 42]. For smooth, homogeneous surfaces, a recent study by Zhao et al. [43] has shown that the temperature at which the vapor layer forms spontaneously from a liquid-solid contact depends only on the hydrophobicity of the surface [43]. For water drops on metallic surfaces, this corresponds to temperatures exceeding 200°C. Yet, we have known for 50 years that water Leidenfrost drops can exist on metal surfaces cooled down to the boiling temperature (100°C) [44].

Here we show how this large metastable region arises from the hydrodynamic stability of the gas flow in the vapor layer. Our experiments employ a new electrical technique that can directly measure the average thickness of the vapor layer around a heated solid. We are able

to monitor the dynamics of the vapor layer’s formation upon heating and eventual collapse upon cooling with microsecond resolution. For smooth metallic surfaces, we find an upper Leidenfrost temperature, T_+ , consistent with recent predictions of a nanoscale wetting theory [43], and a lower Leidenfrost temperature, T_- , which is nearly independent of liquid impurities and solid properties. For a given geometry of the heated solid, the vapor layer thickness is solely a function of the surface temperature. These results are in striking agreement with computer simulations that consider the thermodynamics and hydrodynamics in the liquid, solid, and gas phases, as well as simple theory of lubricating flow in the vapor layer.

Depositing a droplet on a smooth surface below T_+ usually results in liquid-solid contact and nucleate boiling. However, once formed, a small droplet can maintain a stable vapor layer well below T_+ [44]. For example, Fig. 1a shows a levitating water drop on a solid aluminum surface at temperature T_s . As the surface cools, the drop evaporates and remains levitated even below the boiling point of the liquid (Video S1 [45]). Under a larger drop, we expect the vapor layer to collapse at higher temperatures [6]. Thus, in order to investigate the vapor layer stability with fixed geometry, we immersed a metallic cylinder (diameter = 7.9 mm) with a rounded tip into a liquid bath heated to a temperature T_l (Fig.1b). A ceramic heater and thermocouple were embedded in the cylinder, and the bath was heated externally. With this geometry, both T_s and T_l could be controlled.

To study the dynamics of the vapor layer at short time scales, we monitored the electrical impedance between the heated solid and a geometrically-similar lower electrode immersed in the bath. A 10 MHz signal is driven into the lower electrode and the transmitted signal is measured with a PC-based oscilloscope. The amplitude and phase of the signal is extracted by custom software-based lock-in detection (Fig. S1 [45]), as done in similar experiments investigating drop coalescence [46]. We add a variable concentration of NaCl salt to the bath in order to increase the conductivity of the liquid. The region between the two electrodes, shown in the dashed box in Fig. 1b, is modeled as an equivalent circuit of capacitors

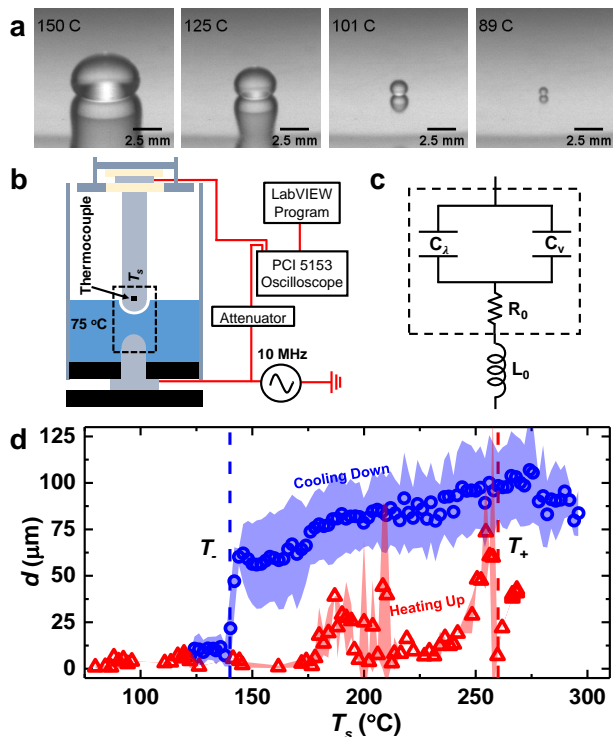


FIG. 1. (a) Sequence of images showing a single pure water Leidenfrost drop that remains levitated over a heated aluminum surface below the boiling point (Video S1 [45]). (b) Experimental setup for high-speed measurements of the vapor layer dynamics. The dashed box indicates the complex impedance which varies in time. (c) Equivalent circuit for the complex impedance of the vapor layer, as described in the main text. Both C_v and C_λ are time dependent. (d) Effective thickness of a pure water vapor layer, d , as a function of the solid surface temperature, T_s , while a nickel-coated copper electrode is first heated (red triangles) and then subsequently cooled (blue circles). $T_+ \approx 260^\circ\text{C}$ (red dashed line) is the average temperature when the vapor layer forms, and $T_- \approx 140^\circ\text{C}$ (blue dashed line) is the average temperature when the vapor layer collapses. The shaded regions show the standard deviation from multiple experiments.

and resistors (Fig. 1c). The inductance, L_0 , represents parasitic inductance in the experimental apparatus. R_0 is the combined resistance of the liquid and metal-liquid boundaries.

The interface between the upper, heated electrode and the liquid is modeled as a parallel combination of two capacitors. C_v is the capacitance of the vapor layer, and C_λ is the capacitance of the double layer that forms upon liquid-solid contact (Fig. S2 [45]). We treat the vapor layer as a capacitor where one plate is the heated metal electrode, and the other is the liquid surface [47]. We can extract the time-dependent thickness of the vapor layer, $d(t)$, by modeling C_v as two concentric hemispheres. The accuracy of this approximation was verified using electro-

static simulations in COMSOL [45, 48].

Upon heating and then cooling the immersed upper electrode, we observed a large, metastable region characterized by hysteresis in d versus T_s . Figure 1d shows the average vapor layer thickness between pure water at $T_l = 75\text{-}95^\circ\text{C}$ and a nickel-coated copper electrode. Only the hemispherical tip of the electrode was immersed in the liquid. While heating, bubble nucleation and detachment resulted in large variations in our measurements of d . For this experiment, NaCl was not added to avoid salt deposition on the electrode surface. On average, a stable vapor layer formed at approximately $T_+ = 260^\circ\text{C}$, which is consistent with recent theoretical predictions for metallic surfaces [43]. Nevertheless, once formed, the vapor layer remained stable at temperatures well below T_+ . As shown in Fig. 1d, the collapse of the vapor layer occurred repeatedly at $T_- = 140^\circ\text{C}$. Video S2 [45] shows a time lapse of a characteristic experiment including the formation and eventual collapse of the vapor layer.

The collapse of the vapor layer at T_- is rapid and explosive, and makes an audible sound. To simultaneously visualize the collapse of the vapor layer during the electrical measurement, we used synchronized high-speed video (Phantom V7.11, Vision Research). The timescale of the collapse was ≈ 3 ms. Figure 2a shows the total impedance of the system before and after a single collapse event. At first, there is a rapid rise in impedance as the liquid touched the surface and an explosive wetting front spread out from the initial contact point (Fig. 2b). The speed of this front is consistent with the capillary velocity, $\gamma/\eta_w \approx 210$ m/s, where $\gamma = 59$ mN/m is the liquid-vapor surface tension and η_w is the viscosity of water at the boiling point. The slower decay in the impedance is due to the dissipation of a large cloud of vapor bubbles (Video S3 [45]). The time evolution of R_0 and $C_v + C_\lambda$ for this experiment are shown in Fig. S3 [45].

For some experiments, prior to the collapse, we observed oscillations in the impedance (Fig. 2a, inset) that we attribute to capillary waves that form and travel upwards along the vapor layer. The existence of waves depends on the amount of the electrode immersed in the liquid. In Video S3 [45], capillary waves are visible with a typical wavelength of $\lambda = 2\text{-}3$ mm. We can estimate the corresponding frequency using the dispersion relation for pure capillary waves, $f = (\gamma k^3 / \rho_l)^{1/2} / 2\pi \approx 120\text{-}220$ Hz, where $\rho_l = 959$ kg/m³ is the density of pure water at the boiling point, and $k = 2\pi/\lambda$ is the wave vector. This agrees well with the inset of Fig. 2a, where $f \approx 200$ Hz.

During the initial moments of collapse when the total impedance increases, the combined capacitance, $C_v + C_\lambda$, increases by more than 3 orders of magnitude (Fig. 2b). The large increase in capacitance is due to the formation of an ionic double layer as soon as the liquid contacts the surface, made possible by the addition of salt in the water. The effective thickness of the ionic screening layer (1-10 nm [49]) is 3 orders of magnitude smaller than the

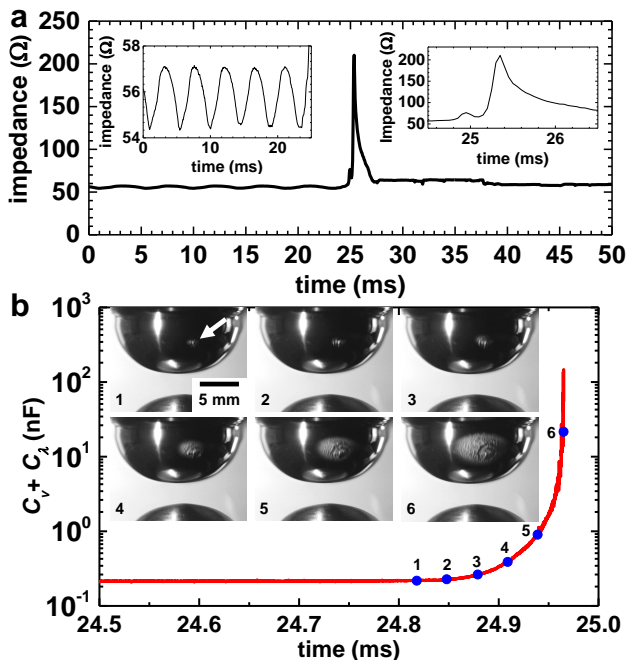


FIG. 2. (a) The total impedance of the Leidenfrost cell, shown in Fig. 1b, during the collapse of a water vapor layer with 0.02 M NaCl. The large spike represents the rapid nucleation of bubbles (Video S3 [45]). Inset: capillary waves are visible in the signal prior to collapse, as described in the text. (b) Total capacitance of the liquid-vapor-solid interface in the initial moments of collapse. The enormous increase is due to the formation of an ionic double layer at the liquid-solid contact. The images show a time sequence of the initial collapse point where bubbles are generated as the wetting front spreads rapidly. The blue points in the data correspond to the indicated images.

thickness of the vapor layer, resulting in a much larger capacitance. Thus, even a small fraction of liquid touching the electrode surface will drastically increase the capacitance (Fig. S2 [45]).

When the vapor layer is present, $C_\lambda = 0$, and the average thickness of the vapor layer can be computed from C_v using a model of concentric spherical shells which are truncated at the height of the water [45]:

$$C_v = 2\pi c H \epsilon_v \frac{R + d}{d}, \quad (1)$$

where R is the radius of curvature of the hemispherical tip of the electrode, H is the height of the water above the tip, and $\epsilon_v = 1.0057\epsilon_0$ is the permittivity of the water vapor at 100°C. The constant $c = 1.051$ is a fitting parameter which accounts for a small discrepancy between the simple capacitor model and a numerical computation of the capacitance (Fig. S4 [45]). In Fig. 2b where $C_v \approx 0.25$ nF prior to collapse, $d \approx 15$ μm.

Surprisingly, and in contrast to the strong dependence of T_+ on material properties [43], we found that T_- was

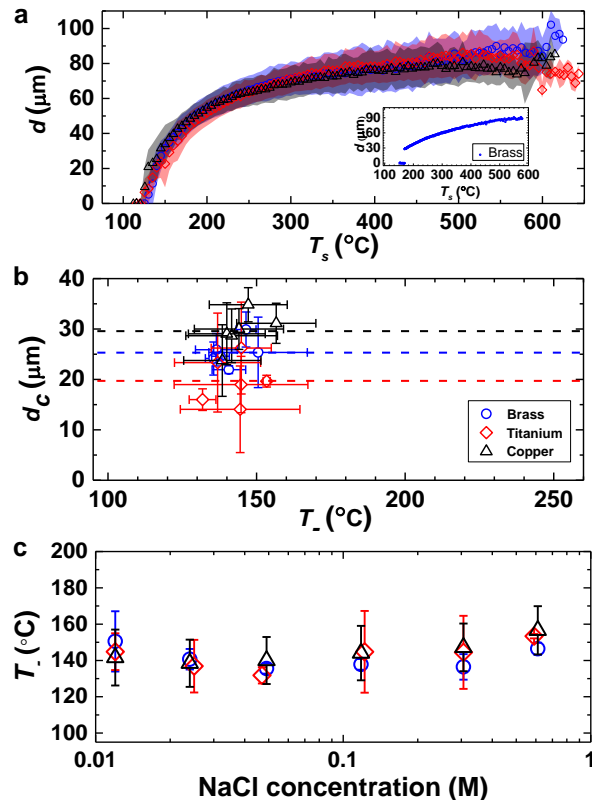


FIG. 3. (a) Average thickness, d , as a function of T_s during cooling with a stable vapor layer. Data are shown for titanium, brass, and copper, with little distinction. The shaded region shows the standard deviation from multiple experiments. Inset: a single cooling curve for a brass experiment. The discontinuity corresponds to vapor layer collapse. (b) Average thickness (d_c) and temperature (T_-) at collapse for the 3 materials. Each data point corresponds to a different concentration of NaCl in the liquid, and error bars represent the standard deviation from multiple experiments. The dashed lines show the mean value of d_c . (c) The same data as in (b), but plotted versus NaCl concentration, confirming little or no dependence.

independent of the metal used in the experiment. Figure 3a shows d versus T_s from multiple experiments of metals with varying thermal conductivities: titanium (7 W/m·K), brass (115 W/m·K), and copper (390 W/m·K). For each material, the time evolution of T_s looked distinct due to differences in heat capacity (Fig. S5 [45]), yet d only depended on T_s . The average thickness d decreased smoothly with T_s until about 140 °C, where the vapor layer spontaneously collapsed. The inset shows a single experiment with brass as the heated electrode, with a discontinuity due to the sudden collapse.

Figure 3b shows the average thickness at collapse, d_c , as a function of T_- . We noticed a slight dependence of the average value of d_c on thermal conductivity, as shown by the dashed lines. A larger thermal conductivity resulted in larger values of d_c . We speculate that this may be re-

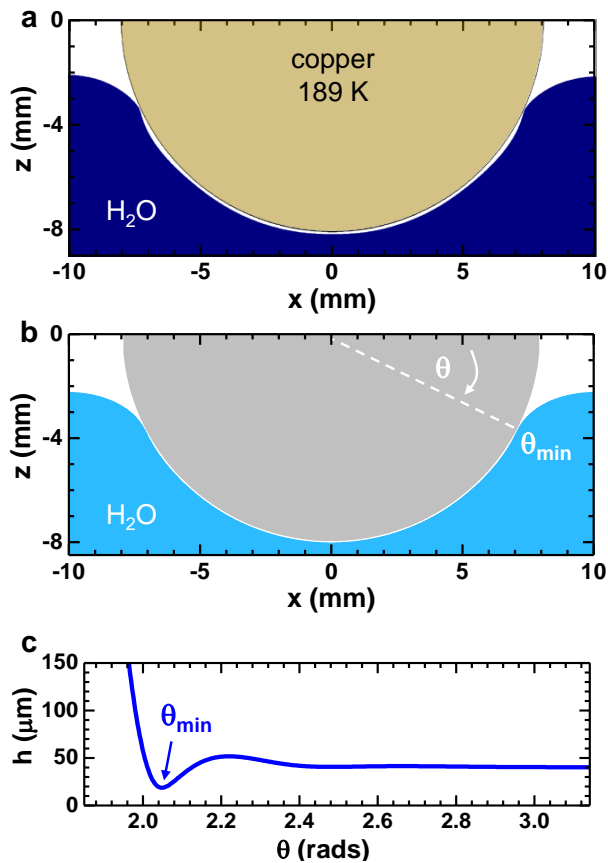


FIG. 4. (a) Model output showing a stable, pure water vapor layer surrounding a hot, copper semicircle in the final moments before collapse. The vapor layer’s time evolution, including thermodynamic and hydrodynamic quantities, were computed using COMSOL [45]. (b) Stable solution of a thin, water vapor layer computed using a viscous lubrication approximation with no thermodynamics [45]. The layer is fed with gas at uniform velocity $v_0 = 0.001$ m/s from the liquid interface. (c) Angular profile of the vapor layer thickness in (b), where θ_{min} denotes the position of minimum thickness.

lated to temperature inhomogeneities near the tip of the electrode. Additionally, the data shown in Fig. 3b represent experiments with various salt concentrations. The addition of salt is known to strongly affect Leidenfrost phenomena [36, 41, 42], despite the fact that NaCl concentrations even up to sea water do not strongly affect the vapor pressure [50], evaporation rate, boiling point, viscosity [51], or the surface tension of water [52]. To investigate this in our experiments, the salt concentration in the liquid was varied between 0.012 M and 0.6 M. For all of our experiments, T_- showed little or no dependence on both thermal conductivity (Fig. 3b) and salt concentration (Fig. 3c).

The experimental data suggest that the lower Leidenfrost temperature (T_-) is determined by the hydrodynamic stability of the vapor layer. Failure occurs when

$d \gtrsim 10 \mu\text{m}$, yet the location and initiation of the collapse may depend on the point of minimum thickness and any associated temporal fluctuations in the vapor layer [3, 14, 15, 30, 53]. In our experiments, collapse consistently occurred away from the tip of the electrode. To understand this behavior, we simulated our system in COMSOL [48] by employing a two-dimensional thermodynamic and hydrodynamic model of the vapor layer (see full description in the supplementary material [45]). The vapor layer is fed by evaporation, and gas is expelled near a point of minimum thickness below the hydrostatic water level. Figure 4a shows a typical model output of a vapor layer between copper and water just prior to collapse. The kink visible at $x \approx 7$ mm is the point of minimum thickness where collapse is initiated (Video S4 [45]). In the simulation, d_c is also independent of the total heat transfer conductivity, but does depend on the surface rate, as evidenced by varying the surface emissivity (Fig. S6 [45]).

A sharp minimum in the layer thickness facilitates a sharp transition from high to low pressure [3, 6–8]. The location of the minimum is almost purely determined by a lubrication approximation of the vapor layer hydrodynamics. We verified this by computing the steady profile of an axisymmetric vapor layer around a hemisphere. The viscous, lubricating vapor layer is fed by a spatially-uniform flow of gas from the liquid interface. The vapor layer profile is defined by its thickness, h , and depth-averaged velocity, \bar{u} , both of which are functions of θ , the polar angle measured from the positive z -axis. Figure 4b shows a steady profile around the hemispherical tip for water. The angular profile, $h(\theta)$, is shown in Fig. 4c, where the minimum indicated thickness matches very well with the COMSOL simulation. Similar agreement is observed for the velocity in the vapor layer (Figs. S6d and S7b [45])

Although material and liquid properties play a leading role in determining the formation temperature (T_+) of a Leidenfrost vapor layer on a smooth surface, here we demonstrated how the failure temperature (T_-) is dominated by the hydrodynamic stability of the lubricating vapor film. These two temperatures can be separated by more than 100°C , leading to a large hysteresis and an explosive collapse at low temperatures. This study inherently poses outstanding questions surrounding the initiation of vapor layer collapse, either through unsteady hydrodynamic fluctuations or surface roughness. The liquid interface must approach the surface on sub-micron length scales for short-ranged van der Waals forces to initiate contact and wetting [43]. We suspect that in highly-dynamic geometries where the vapor layer is constantly in motion, hysteresis may not be visible due to repeated liquid-solid contacts [30]. Nevertheless, this study explains the surprising robustness of Leidenfrost vapor layers once they are formed, and the physics that determines their violent demise.

This work was supported by the NSF DMR Grant No. 1455086.

* justin.c.burton@emory.edu

- [1] J. G. Leidenfrost, *De aquae communis nonnullis qualitatibus tractatus* (Ovenius, 1756).
- [2] D. Quéré, *Annu. Rev. Fluid Mech.* **45**, 197 (2013).
- [3] J. C. Burton, A. L. Sharpe, R. C. A. van der Veen, A. Franco, and S. R. Nagel, *Phys. Rev. Lett.* **109**, 074301 (2012).
- [4] S. B., A. Rednikov, S. Dorbolo, and P. Colinet, *Phys. Rev. E* **90**, 053011 (2014).
- [5] A.-L. Biance, C. Clanet, and D. Quéré, *Phys. Fluids* **15**, 1632 (2003).
- [6] J. H. Snoeijer, P. Brunet, and J. Eggers, *Phys. Rev. E* **79**, 053011 (036307).
- [7] L. Duchemin, J. R. Lister, and U. Lange, *J. Fluid Mech.* **533**, 161 (2005).
- [8] J. R. Lister, A. B. Thompson, A. Perriot, and L. Duchemin, *J. Fluid Mech.* **617**, 167 (2008).
- [9] A. Bouillant, T. Mouterde, P. Bourrienne, A. Lagarde, C. Clanet, and D. Quéré, *Nature Physics* (2018).
- [10] T. R. Cousins, R. E. Goldstein, J. W. Jaworski, and A. I. Pesci, *J. Fluid Mech.* **696**, 215 (2012).
- [11] G. Lagubeau, M. Le Merrer, C. Clanet, and D. Quéré, *Nature Phys.* **7**, 395 (2011).
- [12] H. Linke, B. J. Alemán, L. D. Melling, M. J. Taormina, M. J. Francis, C. C. Dow-Hygelund, V. Narayanan, R. P. Taylor, and A. Stout, *Phys. Rev. Lett.* **96**, 154502 (2006).
- [13] A. Gauthier, C. Diddens, R. Proville, D. Lohse, and D. van der Meer, *Proc. Natl. Acad. Sci. USA* **116**, 1174 (2019).
- [14] X. Ma and J. C. Burton, *Journal of Fluid Mechanics* **846**, 263 (2018).
- [15] X. Ma, J. Liétor-Santos, and J. C. Burton, *Physical Review Fluids* **2**, 031602(R) (2017).
- [16] T. Tran, H. J. J. Staat, A. Prosperetti, C. Sun, and D. Lohse, *Phys. Rev. Lett.* **108**, 036101 (2012).
- [17] G. Castanet, O. Caballina, and F. Lemoine, *Phys. Fluids* **27**, 063302 (2015).
- [18] G. Riboux and J. M. Gordillo, *J. Fluid Mech.* **803**, 516–527 (2016).
- [19] S.-C. Yao and K. Y. Cai, *Exp. Therm. and Fluid Sci.* **1**, 363 (1988).
- [20] C. Bain, *Nature Nanotechnology* **2**, 344 (2007).
- [21] M. Elbahri, D. Paretkar, K. Hirmas, S. Jebril, and R. Adelung, *Advanced Materials* **19**, 1262 (2007).
- [22] V. Lorenz, *Geolines* **15**, 72 (2003).
- [23] L. De León-Barragán, G. Carrasco-Núñez, and M. H. Ort, *Journal of Volcanology and Geothermal Research* **392**, 106789 (2020).
- [24] L. McKeown, M. Bourke, and J. McElwaine, *Scientific reports* **7**, 1 (2017).
- [25] G. G. Wells, R. Ledesma-Aguilar, G. McHale, and K. Sefiane, *Nature communications* **6**, 1 (2015).
- [26] H. Kim, B. Truong, J. Buongiorno, and L.-W. Hu, *Appl. Phys. Lett.* **98**, 083121 (2011).
- [27] S. H. Kim, H. S. Ahn, J. Kim, M. Kaviani, and M. H. Kim, *Appl. Phys. Lett.* **102**, 233901 (2013).
- [28] C. Kruse, T. Anderson, C. Wilson, C. Zuhlke, D. Alexander, G. Gogos, and S. Ndao, *Langmuir* **29**, 9798 (2013).
- [29] H. Kim, J. Buongiorno, L. Hu, and T. Mckrell, *International Journal of Heat and Mass Transfer* **53**, 1542 (2010).
- [30] P. R. Jones, C. Chuang, T. Sun, T. Y. Zhao, K. Fezzaa, J. C. Takase, D. Singh, and N. A. Patankar, *Scientific Reports* **9**, 1598 (2019).
- [31] G. Liu and V. S. J. Craig, *Faraday Discussions* **146**, 141 (2010).
- [32] I. U. Vakarelski, J. O. Marston, D. Y. C. Chan, and S. T. Thoroddsen, *PRL* **106**, 214501 (2011).
- [33] I. Vakarelski, N. A. Patankar, J. O. Marston, D. Y. C. Chan, and S. T. Thoroddsen, *Nature* **489**, 274 (2012).
- [34] R. Freud, R. Harari, and E. Sher, *Nuclear Engineering and Design* **239**, 722 (2009).
- [35] V. V. Yagov, A. R. Zabiroy, and M. A. Lexin, *Heat and Mass Transfer and Properties of Working Fluids and Materials* **62**, 833 (2015).
- [36] S. Hsu, Y. Ho, M. Ho, J. Wang, and C. Pan, *International Journal of Heat and Mass Transfer* **86**, 65 (2015).
- [37] I. Sher, R. Harari, R. Reshef, and E. Sher, *Applied Thermal Engineering* **36**, 219 (2012).
- [38] H. Jouhara and B. P. Axcell, *Nuclear Engineering and Design* **239**, 1885 (2009).
- [39] V. V. Yagov, M. A. Lexin, A. R. Zabiroy, and O. N. Kaban'kov, *International Journal of Heat and Mass Transfer* **100**, 908 (2016).
- [40] W. S. Bradfield, *Ind. Eng. Chem. Fundamen.* **5**, 200 (1966).
- [41] C.-K. Huang and V. P. Carey, *International Journal of Heat and Mass Transfer* **50**, 269 (2007).
- [42] K. H. M. Abdalrahman, Sabariman, and E. Specht, *International Journal of Heat and Mass Transfer* **78**, 76 (2014).
- [43] T. Y. Zhao and N. A. Patankar, *PNAS* **117**, 13321 (2020).
- [44] K. J. Baumeister, R. C. Hendricks, and T. D. Hamill, *NASA Technical Note D3226* (1966).
- [45] See Supplemental Material at [URL will be inserted by publisher] for videos and a detailed description of the experiments and simulations.
- [46] J. D. Paulsen, J. C. Burton, and S. R. Nagel, *PRL* **106**, 114501 (2011).
- [47] T. Roques-Carmes, A. Dompes, P. Marchal, and L. Marchal-Heussler, *Experiments in Fluids* **59**, 115 (2018).
- [48] COMSOL Multiphysics®, v. 5.3. COMSOL AB, Stockholm, Sweden (2020).
- [49] M. Khademi and D. P. J. Barz, *Langmuir* **36**, 4250 (2020).
- [50] B. M. Fabuss and A. Korosi, *Desalination* **1**, 139 (1966).
- [51] J. Kestin, H. E. Khalifa, and C. R. J., *Journal of Physical and Chemical Reference Data* **10**, 71 (1981).
- [52] G. Jones and W. A. Ray, *J. Am. Chem. Soc.* **63**, 3262 (1941).
- [53] T. A. Caswell, *Physiscal Review E* **90**, 013014 (2014).